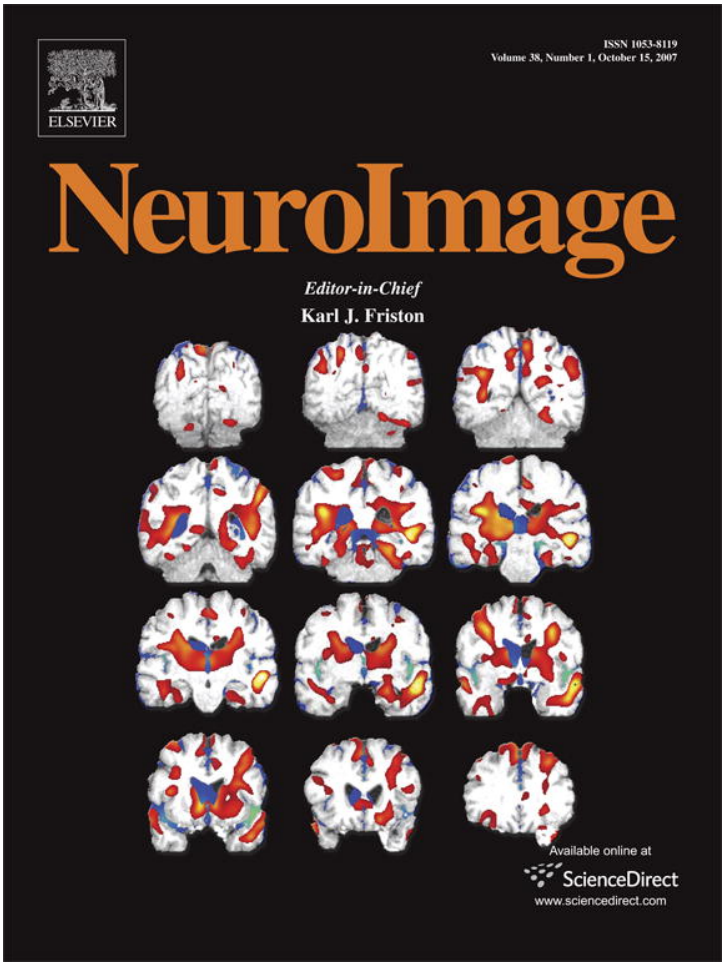

ELSEVIER

NeuroImage

www.elsevier.com/locate/ynimg
NeuroImage 38 (2007) 138–149

Short-term changes in bilateral hippocampal coherence precede epileptiform events

Ralph Meier,[a,b,*,1] Ute Häussler,[a,b,c,1] Ad Aertsen,[a,b] Colin Deransart,[c] Antoine Depaulis,[c] and Ulrich Egert[a,b]

[a] *Bernstein Center for Computational Neuroscience Freiburg, Hansastrasse 9a, 79104 Freiburg, Germany*
[b] *Neurobiology and Biophysics, Faculty of Biology, Albert-Ludwigs-University, Schänzlestrasse 1, 79104 Freiburg, Germany*
[c] *U836 Inserm-Université Joseph Fourier-CEA, 2280 Rue de la Piscine, BP 38041 Grenoble Cedex 9, France*

Received 16 April 2007; revised 6 June 2007; accepted 20 July 2007
Available online 1 August 2007

The mesial temporal lobe epilepsy syndrome (MTLE) is the most common form of focal epilepsies. MTLE patients usually respond very little to pharmacological therapy and surgical resection of temporal brain areas is mandatory. Finding less invasive therapies than resection of the sclerotic hippocampus requires knowledge of the network structures and dynamics involved in seizure generation. Investigation of the time interval immediately preceding seizure onset would help in understanding the initiation mechanisms of the seizure proper and, thereby, possibly improve therapeutical options. Here, we employed the *in vivo* intrahippocampal kainate model in mice, which is characterized by unilateral histological changes, resembling hippocampal sclerosis observed in human MTLE, and recurrent focal seizures. In these epileptic mice, population spikes occurred during epileptiform events (EEs) in the ipsilateral, histologically changed hippocampus, but also concomitantly in the contralateral, intact hippocampus. We studied synchronization processes between the ipsilateral, sclerotic hippocampus and the contralateral hippocampus immediately preceding the onset of EEs. We show that coherence between the two hippocampi decreased consistently and reliably for all EEs at 8 to 12 s before their onset at high frequencies (>100 Hz), without changes in power in these bands. This early decoupling of the two hippocampi indicates the time range for cellular and network mechanisms leading to increased excitability and/or synchronicity in the tissue and thus ultimately to epileptic seizures.

Introduction

The mesial temporal lobe epilepsy syndrome (MTLE) is the most common form of focal epilepsies (Cendes et al., 2002). It is associated with severe changes in hippocampal histology, termed hippocampal sclerosis (Engel, 1996; Wieser, 2004; Chabardes et al., 2005), and recurrent seizures occur mostly confined to temporal brain regions. MTLE responds poorly to pharmacological therapy and, thus, surgical resection of the involved brain areas is necessary to suppress seizures (Engel, 1996; Chabardes et al., 2005). Improvement of therapeutic options requires a better understanding of the mechanisms involved in the emergence of seizures, with respect to both network and temporal structure. It is, thus, important to know whether the sclerotic area of the hippocampus is the only brain area involved in seizure generation, or if the interaction with "intact" areas is required. In rodents, the two hippocampi are closely interconnected via hilar cells (Laurberg and Sorensen, 1981; Ribak et al., 1985; Frotscher et al., 1991; Deller et al., 1995) and CA3 pyramidal cells (Swanson et al., 1978). Coherence of activity at theta (6–10 Hz) and gamma frequencies (~40–100 Hz) shows a high synchronization between the hippocampi under physiological conditions (Buzsaki et al., 2003). This could allow interhippocampal interaction to contribute to seizure initiation.

EEG analyses in human MTLE found desynchronization within each hippocampus, but also between both hippocampi, many minutes to hours before seizure onset (Mormann et al., 2003). However, there is a large variability how early an upcoming seizure can be detected across patients within this but also across different studies (Mormann et al., 2007). This makes it difficult to interpret the cellular and network mechanisms contributing to seizure initiation, whose investigation is very limited in humans. To overcome this limitation, it is important to understand basic mechanisms of seizure emergence (ictogenesis) in validated animal models.

Here, we investigated interhippocampal synchronization immediately preceding spontaneous epileptiform events (EE) to reveal processes involved in their generation on a short time scale. We used the model of intrahippocampal kainate in mice that reproduces several features of human MTLE (Suzuki et al., 1995;

* Corresponding author. Bernstein Center for Computational Neuroscience Hansastr. 9A, 79104 Freiburg i.Br., Germany. Fax: +49 761 203 9559.
E-mail address: meier@biologie.uni-freiburg.de (R. Meier).
[1] Both authors contributed equally to this work.
Available online on ScienceDirect (www.sciencedirect.com).

1053-8119/$ - see front matter © 2007 Elsevier Inc. All rights reserved.
doi:10.1016/j.neuroimage.2007.07.016

Bouilleret et al., 1999; Riban et al., 2002). In these mice a single unilateral injection of kainic acid into the hippocampus first induces a status epilepticus lasting for up to 15 h. Then, during the next 2 weeks recurrent spontaneous hippocampal discharges progressively develop to become stable for the lifetime of the animals. These focal seizures occur mainly during rest, only rarely generalize to the cortex and are resistant to most antiepileptic drugs (Riban et al., 2002). The histological changes resemble human hippocampal sclerosis, including cell death in CA1, CA3 and the hilus, sprouting of mossy fibers, gliosis and, in particular, dispersion of the granule cells (Suzuki et al., 1995; Heinrich et al., 2006). At the stage investigated in the current study, all these changes are pronounced in the injected hippocampus, but are not conspicuous in the contralateral hippocampus. A more detailed analysis of the anatomical changes in the contralateral hippocampus has not been carried out, yet.

To detect long-range synchrony between the injected and the contralateral hippocampus, we analyzed coherence in simultaneously recorded local field potentials (LFP). We show that coherence between the hippocampi decreased significantly and consistently across all EEs from different mice already at 8–12 s before EE onset, indicating a time span in which essential seizure initiation mechanisms take place.

Methods

Animals

Adult male C57Bl/6 mice, aged 8–12 weeks (Janvier, Le-Genest-St-Isle, France) were used in this study. After surgery, they were housed in individual cages with food and water ad libitum in a 12-h light/dark cycle. Experimental procedures and animal care were carried out in accordance with the European Community Council Directive of 24 November 1986 (86/609/EEC). They were approved by the ethical committee in charge of animal experimentation at the University Joseph Fourier, Grenoble, France (number 89-06).

Kainate injection and electrode implantation

Mice were anesthetized (chloral hydrate, 0.4 g/kg, i.p.) and placed into a stereotaxic frame in flat skull position. Body temperature was maintained with a heating blanket. Kainate injections were performed as described previously (Heinrich et al., 2006). Briefly, a stainless steel cannula was connected via tubing to a 0.5-µl micro-syringe (Hamilton, Bonaduz, Switzerland) and filled with 20 µM kainic acid solution (Sigma, Lyon, France) in 0.9% NaCl. The cannula was positioned in the right dorsal hippocampus (coordinates from bregma: anterioposterior [AP]=2.0 mm, mediolateral [ML]=1.5 mm, dorsoventral [DV]=2.0 mm) and 50 nl (1 nmol) of kainic acid solution were injected during 1 min using a micro-pump (CMA/100, Carnegie Medicine, Stockholm, Sweden) to drive the micro-syringe. After injection, the cannula was left in place for 2 min to avoid reflux. Subsequently, custom-made wire electrodes (stainless steel, Ø 0.125 mm, polyester insulated) were implanted with cortical electrodes consisting of one wire and hippocampal electrodes consisting of two twisted wires with a vertical tip separation of 0.3–0.5 mm. Hippocampal electrodes were implanted into both hippocampi at mirrored coordinates (AP −2.0, ML −1.5/+1.5, DV −1.9, relative to bregma). Cortical electrodes were implanted in both hemispheres in the frontal cortex (frontal to bregma) with only the tip (0.5 mm) protruding into the cortical tissue. The reference electrode was placed over the vermis of the cerebellum; two ground electrodes were fixed to the skull over the cerebellum and cortex, respectively. All electrodes were fixed to the skull with cyanoacrylate and dental acrylic cement. Electrodes and connectors were stable for several months. After recovery from anesthesia a transient status epilepticus of 6–12 h was observed, as previously described (Heinrich et al., 2006). This status epilepticus subsided spontaneously. Of the 13 mice injected 8 had developed EE as defined below at 4 weeks after injection and were used in this study. In all these mice histological changes were found as shown in Fig. 1.

Electrophysiological recordings

Mice were recorded in a plexiglas box, where they could freely move. A miniature headstage preamplifier (11 channels, MPA8I, Multi Channel Systems, Reutlingen, Germany) was directly connected to the mouse's head to minimize movement artefacts. LFPs were amplified, filtered (system amplification 2000×, system bandpass 1 Hz–5 kHz; FA32I, Multi Channel Systems) and stored to hard disk (16-bit ADC, 20-kHz sampling frequency; CED Power1401, CED, Cambridge, UK) using the Spike2 software. The recordings analyzed in this study were obtained at least 6 weeks after kainate injection. After adaptation to the recording cage, mice

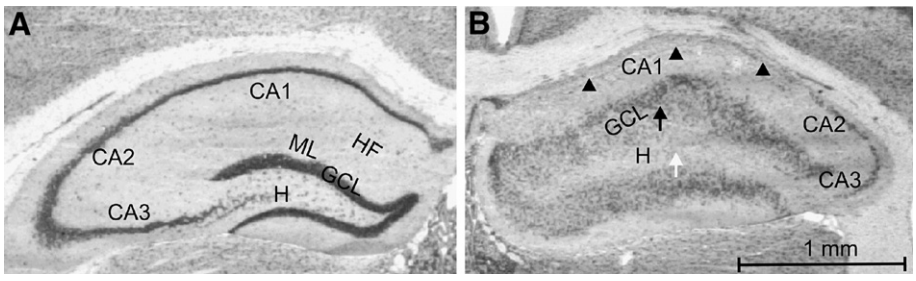

Fig. 1. Hippocampal sclerosis after injection of kainate occurred only in the ipsilateral hippocampus. Coronal sections of the hippocampus contralateral (A) and ipsilateral (B) to the injection site were stained with cresyl violet acetate. (A) The contralateral, uninjected hippocampus served as a control, showing normal hippocampal histology. Hippocampal electrodes were located in the hippocampal fissure (HF) or in the molecular layer (ML). (B) In the ipsilateral, injected hippocampus (6 weeks after injection) severe granule cell dispersion (black arrow) was visible. Additionally, pyramidal and inhibitory cells were lost, especially in CA1 (black arrowheads) but also in CA3. Cell loss was also observed in the hilus (white arrow). Only recording data from mice showing this typical pattern were selected for further analysis. Electrodes were all located in the molecular layer or granule cell layer, due to its wide dispersion. Scale bar=1 mm. GCL, granule cell layer; H, hilus; HF, hippocampal fissure; ML, molecular layer.

were recorded for one to three periods of 20 min each. The average interval between recording sessions was 3 days.

Histology

After 2 months, KA mice were injected with a lethal dose of pentobarbital (Dolethal, 100 mg/kg, i.p., Vetoquinol, France). Their brains were extracted, frozen in isopentane (Sigma, Lyon, France) and cut into 20-µm coronal sections on a cryostat. Sections of all mice were stained with cresyl violet acetate and verified for cell loss and granule cell dispersion (Fig. 1). Locations of the recording sites were determined from the same sections.

Event selection

LFP recordings were visually inspected and all EEs were marked in the trace from the ipsilateral hippocampus. EEs were defined when spikes exceeded the baseline amplitude at least three-fold (Figs. 2A–C, black arrows). Population spikes separated by more than 0.5 s were considered as two distinct EEs (Fig. 2). Onset markers were set at the first detectable deviation from baseline for spikes matching the aforementioned criteria, thus including all population spikes into the EE. The time point 0 in all following analyses and plots matches the point of this detected onset. The same criteria were applied to define EE offset (examples see Fig. 2). Two different types of events were selected: 'short EEs' were defined as EEs with a duration between 1 s and 2 s, whereas 'long EEs' lasted longer than 10 s. Short and long EEs where chosen to relate phase synchronization changes to severity (i.e., expressed by their duration) of EEs. EEs of 2 s were long enough to reliably measure low-frequency content. The minimal duration of 10 s for long EEs was chosen to clearly separate them from short EEs and for comparability EEs termed seizures in previous reports (Riban et al., 2002; Heinrich et al., 2006). EEs between 2 s and 10 s were disregarded for this analysis. To determine which hippocampus first exhibited changes in the LFP related to EE onset we calculated the cross-correlation between the raw LFPs recorded simultaneously in the ipsi- and contralateral hippocampi (using Matlab, The Mathworks, Natick, USA). We used cutouts of 2 s before and 2 s after EE onset and calculated the mean coefficient of correlation ±1 standard deviation (SD) for sliding windows of 2 s width (shifted by one data sample (50 µs) each, Fig. 2E).

To ensure a stable baseline preceding EE onset, only EEs without preceding EEs in a time window of at least 20 s were considered (Fig. 3). These criteria were met for 34 short EEs and 45 long EEs (Table 1). In our analyses, we focused on potential

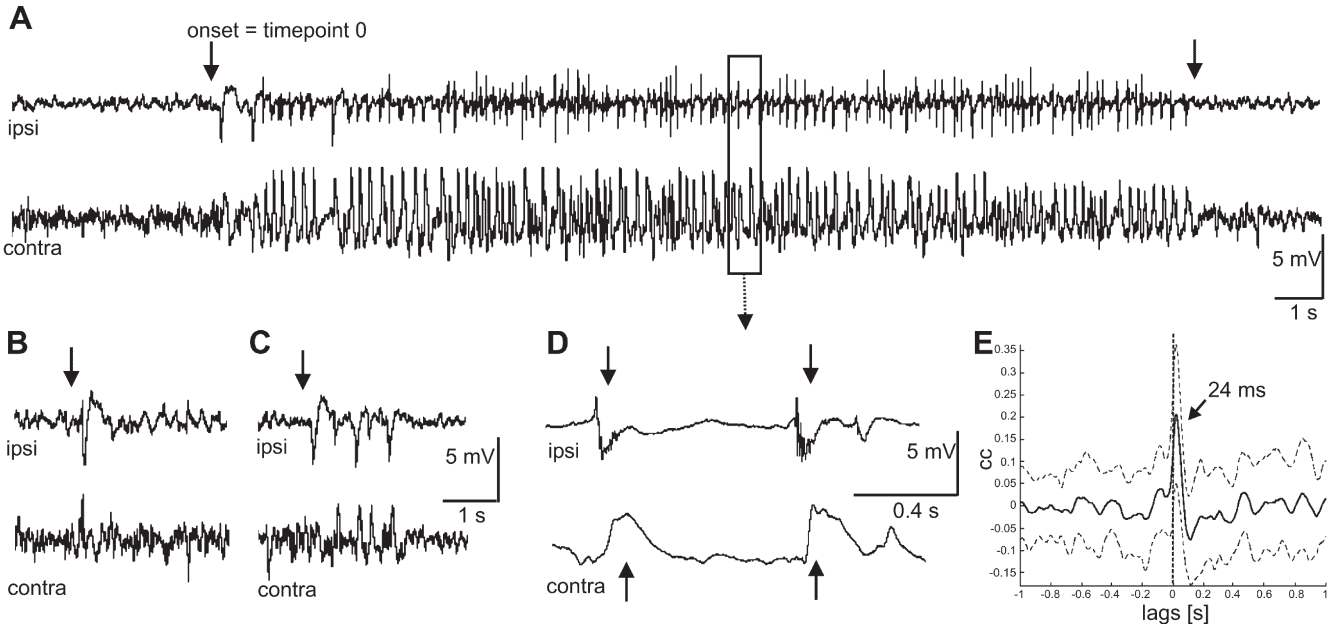

Fig. 2. LFP recordings of hippocampal activity show epileptiform activity. Voltage was measured relative to a reference electrode placed over the vermis of the cerebellum. Population activity recorded from one electrode in the ipsilateral, injected hippocampus (upper trace, A–D) and one electrode in the contralateral, uninjected hippocampus (lower trace, A–D) is shown. (A) The onsets and ends of all EEs were detected manually (arrows) and those lasting longer than 10 s were selected and summarized as long EEs in the analysis (N=45). In all further analyses and plots (Figs. 3–6), this onset is indicated as 0 on the x-axis. These EEs typically started in the ipsilateral hippocampus (upper trace) with a few spikes of high amplitude (onset at arrow), followed by spikes of slightly smaller amplitude but higher frequency. Epileptiform spikes in the ipsilateral hippocampus consisted of population spikes of negative polarity with ripples or FR riding on the peak and ascending phase (enlarged in D, upper trace). Note the occurrence of concomitant spiking in the histologically unchanged contralateral hippocampus (A, lower trace). Population spikes in the contralateral hippocampus lacked any superimposed high-frequency activity (enlarged in D, arrows in lower trace). Signal to noise ratios in the recording from the contralateral hippocampus varied across mice (scale bar 5 mV, 1 s). (B, C) Besides long EEs, epileptiform activity consisted of single spikes (B) or a few grouped spikes (C) of variable, but shorter duration than in long EEs. Among those, only EEs with duration longer than 1 s but shorter than 2 s were selected (short EEs). As in panel A, these EEs occurred mostly concomitantly in both hippocampi. The epileptiform spikes resembled those described in panels A and D (scale bar 5 mV, 0.4 s). (E) Cross-correlation analysis revealed a delayed onset of EEs in the contralateral hippocampus, indicated by a shifted "central" peak towards positive lags (with a median lag of the "central" peak at 24 ms after ipsilateral EE onset for individual EEs).We used raw LFP data cutouts of 1 s before and 1 s after EE onset. The mean coefficient of correlation (solid black)± 1 SD (dashed) is shown, the vertical dotted line indicates 0-ms lag.

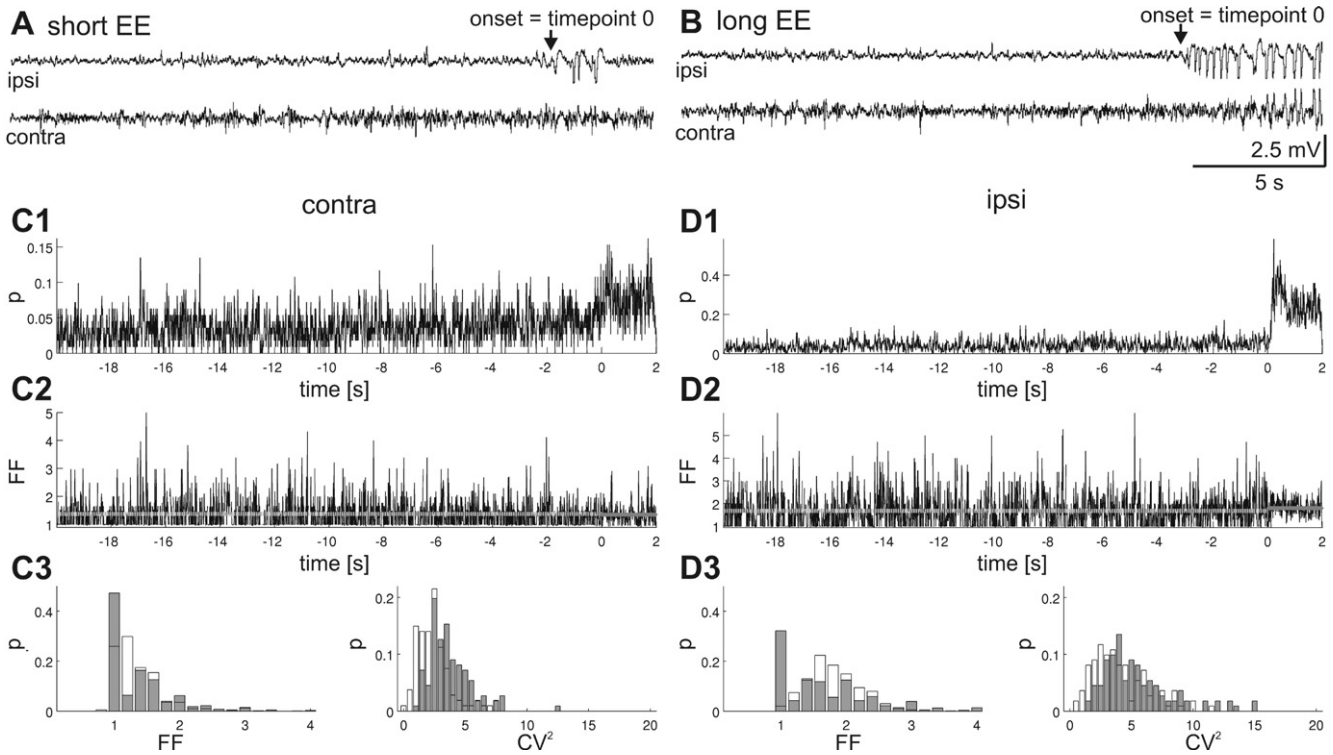

Fig. 3. Short and long EEs could not be anticipated directly from visible cues in the preceding LFP activity. Panels A and B show recordings from electrodes in the hippocampus ipsilateral (upper trace) and contralateral (lower trace) to the injection site, respectively. For analysis we included only such EEs that were preceded by an EE-free period of at least 20 s, similar to the example shown here. (A) The baseline preceding the manually detected onset (black arrow) of a short EE was characterized by low amplitude, arrhythmic activity, occurring in both the ipsilateral (upper trace) and contralateral (lower trace) hippocampus. In the raw data, there were no hints pointing towards the occurrence of an EE in any of the selected EEs. (B) Activity preceding the onsets (arrow) of long EEs, shown here, did not differ from that preceding short EEs (A) (scale bar 2.5 mV, 5 s). (C1, D1) Time-resolved probability for the observation of a spike event in the LFP. Firing rate remained low and unstructured preceding EE onset and increased after EE onset for both hippocampi, especially in the ipsilateral (D1) hippocampus. This demonstrates also the amount of spikes that propagated from the ipsilateral to the contralateral hippocampus during the EE. (C2, D2) The time-resolved Fano Factor (FF) is shown as a measure of firing synchrony over EEs. (C3, D3) A histogram of these values for the time preceding EEs (gray bars) and after EE onset (white bars). We found no prominent synchrony and regularity patterns in the time span preceding EEs. Higher levels of synchrony and regularity are only reached during EEs.

reflections of mechanisms and changes in the network dynamics prior to onset of EEs that can occur within the chosen time window.

To ensure an unbiased, event-free time span preceding EE onset, we confirmed that the detected EE onset was not preceded by any changes in the occurrence patterns of single spikes (Figs. 3C1–D3). First, we detected sharp transients in the LFP by a threshold crossing algorithm. The threshold was set to be 4 times the median of the rectified LFP for the full time span preceding EE onset, in accordance to Quiroga et al. (2004). We then calculated the squared coefficient of variation (CV^2) to measure the regularity of the spike events before and during the EEs. In addition, the Fano Factor (FF) (Fano, 1947, Rieke et al., 1997) was calculated as a characteristic measure for interval distributions in point processes (bin width 200 ms). The overall synchronization of spike events was determined for short and long EEs aligned to EE onset. Moreover, we calculated the time-resolved probability for the occurrence of spikes in 200-ms time bins.

Table 1
Overview of the EE data epochs recorded in this study

Selection types	No. of mice (*N*)	No. of EEs	Average EEs per mouse±SD
Short EEs	7	34	2.6±1.9
Long EEs	7	45	3.5±2.3
Total available	8	641	80±29

We analyzed recordings from 8 animals and selected a subset of EEs, based on visual inspection and the duration of those EEs: EEs with a maximum duration of 2 s, termed ‘short EEs’ and ‘long EEs’ lasting at least 10 s. Furthermore, the EE-free period (i.e., the time preceding a selected EE without any observable artefact or other EE) needed to be at least 20 s. EEs in one animal did not fit the criteria and these recordings were, thus, discarded. The ‘Total available’ row counts all EEs observed in the data, irrespective of their duration or preceding EE-free period.

Spectral and coherence analysis

The EE initiation phase was analyzed from 20 s preceding, and to illustrate the effects of the actually occurring EEs, to 5 s after EE onset. To obtain time-resolved values, spectral and coherence analyses were calculated (using Matlab) for sliding time windows of 1 s, shifted by 0.2 s at a time. The average power spectral density in the frequency range between 1 Hz and 2 kHz was calculated for each hippocampal recording electrode and each

window (Fig. 6). Additionally, the coherence was analyzed using the Matlab function 'mscohere' (Signal Processing Toolbox) which calculated the magnitude squared coherence – defined as the cross power spectral density function normalized by individual auto-power spectral density functions – between all possible electrode pairs. From here on we will refer to this measurement as coherence. To calculate the time-resolved coherence estimate, in agreement with Priestley (1982) and Chatfield (1999), we used a sliding window of 1-s duration, moved by 0.2 s at a time. In each of these time windows we used the following parameters for the calculation of coherence: the number of bins for the fast Fourier transform (FFT) was set to 2^{15} points and we used periodic Hamming windowing with a window length of 0.125 s and 50% overlap. We thus obtained a phase synchronization measure (Nunez et al., 1997; Nunez et al., 1999; Rappelsberger et al., 1994) as a function of frequency aligned to EE onset. We defined a 2-s time window ranging from 20 s to 18 s preceding EE onset as a baseline and subtracted the average baseline coherence from the actual coherence traces. Thus, we show changes of coherence with respect to this baseline. For the coherence estimates in the specific frequency bands we calculated the mean for all frequency bins falling into the given frequency range. To aid visual representation the coherence traces were subsequently smoothed over time by a simple 1-s wide sliding average window.

Hierarchical clustering

Since (temporal) significance estimates for spectral data are notoriously difficult (Chatfield, 1999) we used a multivariate analysis of variance (MANOVA) based single-link clustering method (Krzanowski, 1988; Jain et al., 1999) using the Euclidian distance between the power spectral density of time bins relative to EE onset. MANOVA is an extension of analysis of variance (ANOVA) methods to cover cases where there is more than one dependent variable (here, the power in different frequency bins) and where the dependent variables cannot be combined in a straight forward manner. As well as identifying whether changes in the independent variables (here, the 1-s wide time bins) have a significant effect on the dependent variables, the technique also seeks to identify the interactions among the independent variables and the association between dependent variables, if any. With this approach we can represent the data in a way to reveal possible hidden temporal structures relative to EE onset over all frequency bands. Thus, we derive single-linked hierarchical trees to show similarities in the frequency space between different time bins of the LFP relative to EE onset. The group centers for clustering the data were defined as 1-s wide time bins relative to EE onset. This method shows the relationship and similarity of the power spectral density between the time bins preceding and during an EE. The structure of this hierarchical clustering tree reflects potential correlations of power spectral similarity between EE time bins. Spectral power was calculated for sliding windows of the same extent and slid as described above for frequency bands of 8 to 16, 16 to 32, …, 1024 to 2048 Hz. We analyzed data from 19 s before to 4 s after EE onset. High similarity between the aforementioned time bins was indicated by small inter-group distances, i.e., by short vertical lines ('branches') between the respective labels (x-axis), low similarity by long vertical lines (Fig. 7). Clusters were then defined by gradually decreasing a linear threshold from the maximal group-wise distance (high values on the y-axis) towards zero distance. Such a threshold will identify groups with similar properties. Generally, a small group distance will show high similarity and leads to an assignment of one cluster.

Results

In vivo LFP recordings from 7 mice with loss of neurons in CA1, CA3 and in the hilus, and granule cell dispersion were used for analysis (Table 1 and Fig. 1). In all cases these histological features were limited to the injected hippocampus. No changes were observed in the contralateral hippocampus, in agreement with previous reports (Bouilleret et al., 1999; Riban et al., 2002; Heinrich et al., 2006). In the ipsilateral hippocampus of all mice, the bipolar electrodes were located in the molecular layer (upper tip) and granule cell layer (lower tip), or both in the dispersed granule cell layer. In the contralateral hippocampus, the bipolar electrodes were located in the hippocampal fissure, or in the upper molecular layer (upper tip) and lower molecular layer (lower tip) directly adjacent to the granule cell layer. The electrodes were initially implanted at the same coordinates and depth in both hippocampi; the difference with relation to the cell layers is due to the dispersion of the granule cell layer together with a decreased size of CA1 because of cell loss in the ipsilateral hippocampus after kainate injection.

Involvement of the contralateral hippocampus in epileptiform events

Intrahippocampal LFP recordings and monitoring of the mice 6–10 weeks after the kainate injection showed that short and long EEs occurred mainly during rest without observable motor activity. However, in a few cases, mild chewing movements were observed. Short EEs consisted of single or a few grouped population spikes (Figs. 2B, C) and occurred alternating with long EEs, generally starting with high amplitude spikes, which then decreased in amplitude and slightly increased in frequency (Fig. 2A), as reported previously (Riban et al., 2002). Epileptiform spiking lasted for up to 1 min. EEs in the ipsilateral hippocampus consisted of large, negative, hypersynchronized spikes with fast ripples (FR) of low amplitude riding on the ascending phase and peak (Fig. 2D).

Epileptiform population spikes were not confined to the ipsilateral hippocampus, but concomitantly occurred in the contralateral hippocampus (Figs. 2A, C, D, lower traces), which was histologically unchanged. The relation between spike amplitudes and background activity amplitude varied across mice. However, EEs in the contralateral hippocampus did not occur independently from the ipsilateral one, indicating that there was no formation of a mirror focus. The epileptiform spikes during the EE occurred in the contralateral hippocampus with a short delay after spikes in the ipsilateral hippocampus (average 24 ms as indicated by cross-correlation analysis, Fig. 2E), but were of opposite polarity and did not contain any superimposed ripple activity (Figs. 2A–D, lower traces). The spike amplitude was larger in the hippocampal fissure or upper molecular layer than in the lower molecular layer or granule cell layer. Preceding the onset of EEs no changes in the LFP activity could be observed, thus, the raw data did not give any indications for an upcoming short or long EE (Figs. 3A, B).

To determine if firing probability for single spikes in the LFP changed before EE onset, which could influence our further analysis, we obtained measurements for synchrony (over trials) and irregularity (over time) for these spike events. We demonstrate that

there were no structural changes in the spike event occurrence probability preceding EE onset for both, the ipsi- and contralateral hippocampus (Figs. 3C1, D1). The occurrence probability for spike events increased dramatically with EE onset, as expected by visual impression. The time-resolved FF as a measure for event synchrony over trials did not show any clear structure preceding EE onset, but changed significantly with EE onset for both hippocampi (Figs. 3C2, D2). The distributions of the CV^2 and FF (panels C3, D3) confirmed these observations a highly significant change between the distribution before and after EE onset ($p<0.001$, Wilcoxon rank order test). To summarize, we could not observe changes in the patterns of single spike occurrence preceding EE onset.

Interhippocampal coherence changes before the onset of epileptiform events

To assess the frequency-resolved coupling between oscillatory activities in both hippocampi we calculated coherence for four frequency bands: A broad theta-band (4–13 Hz), gamma-band (40–80 Hz), ripples (100–250 Hz), and FR (200–400 Hz). We chose these bands to include the overlapping definitions of ripples (100 Hz to 200–250 Hz) and FR (200–250 Hz up to 600 Hz) according to Bragin et al. (1999) and Traub (2003). Here, 400 Hz was chosen as a maximum, because FR power in our LFP recordings was highest around 300 Hz and clearly diminished towards 400 Hz. The average coherence in a window between 20 s

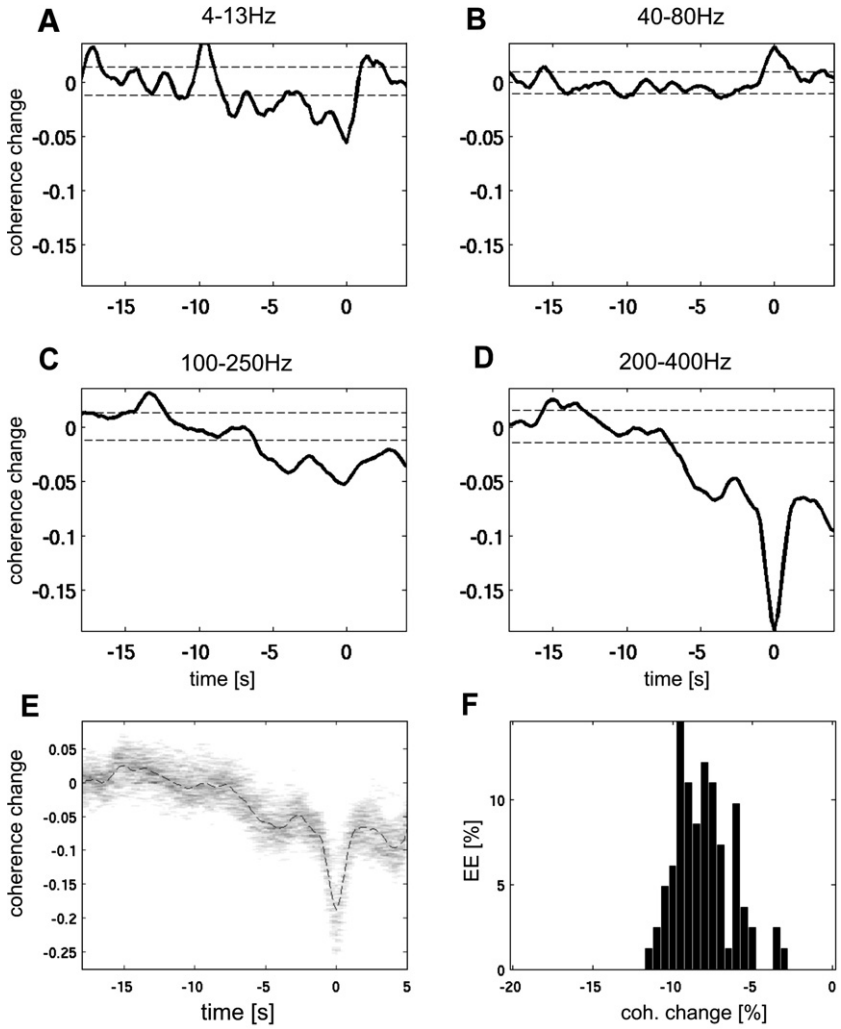

Fig. 4. Time-resolved relative coherence changed several seconds before the onset of short EEs. (A–D) Averaged coherence time course relative to baseline in the theta (4–13 Hz, A), gamma (40–80 Hz, B), ripples (100–250 Hz, C), and FR (200–400 Hz, D) frequency bands. Data traces were smoothed with a 1-s sliding average. The average baseline (−20 s to −18 s) coherence was subtracted from the traces. The dashed lines show 1 SD of the traces in the baseline window to indicate expected variability of the data traces under normal conditions. Time point 0 s denotes the onset of the first spikes of the EEs, as indicated in Figs. 2 and 3, negative *x*-values thus precede the onset of the EE. A prominent decrease of coherence preceding EE onset occurred at high frequencies (C, D), crossing a 1 SD threshold several seconds before EE onset (8±2 s for FR, D). (E) Reliability of the pre-EE coherence decrease for all short EEs. Gray levels correspond to the number of EEs showing a given decrease in the corresponding time window, thus, representing a time-resolved histogram of the individual coherence traces for FR bands. The dashed line shows the mean (as in D). The decrease of coherence at FR frequencies was similar for all short EEs across all 7 mice. (F) Percentage of EEs plotted against the decrease of coherence compared to baseline coherence at 1 s before EE onset. All EE onsets were preceded by a decrease of coherence, the degree of decrease was approximately normally distributed around a mean of 8% (SD 1.8%).

and 18 s before EE onset was taken as baseline and this value was subtracted from the coherence in each window. As a consequence, negative values indicate coherence smaller than baseline, whereas positive values correspond to increased coherence. Time-resolved coherence averaged across all mice illustrates the temporal development of phase-synchronization relative to the onset of short (Figs. 4A–F) and long EEs (Figs. 5A–F). We analyzed coherence for all pairings of ipsi- and contralateral hippocampal electrodes. Since the results were comparable for all pairings, only the data for the lower tip of the electrode ipsilaterally and the upper tip contralaterally will be shown here. Furthermore, amplitudes of epileptiform spikes were largest there.

For short EEs, the time course of coherence in the theta range showed high variability during the 20 s preceding the onset (Fig. 4A). Transient decreases of coherence exceeding the significance threshold of 1 SD occurred preceding EE onset and were followed by an increase of coherence, crossing the threshold at EE onset. In the gamma range no significant changes could be observed before EE onset (Fig. 4B), and only a small, short lasting increase of coherence occurred at EE onset. In contrast, at high frequencies (>100 Hz), coherence showed a striking decrease preceding the onset of EEs (Figs. 4C, D). In the ripple frequency range, coherence decreased at about 6 s before EE onset and remained clearly below the significance threshold before and during the EE (Fig. 4C). This decrease of coherence was even more pronounced in the FR range, crossing the significance threshold at 8±2 s before the EE onset. An additional large decrease could be observed slightly preceding the EE onset, lasting as long as the EE duration (<2 s), and increasing again after EE offset. The fact that this decrease slightly preceded the onset (at time point 0 s) was likely caused by slight misalignment of different EE onsets by less than 1 s, which we will address in the following section. This development of coherence in the FR range held true for each of the EEs selected (Fig. 4E) and is, thus, reliable across mice. Moreover, the percentages of the decrease of coherence across EEs

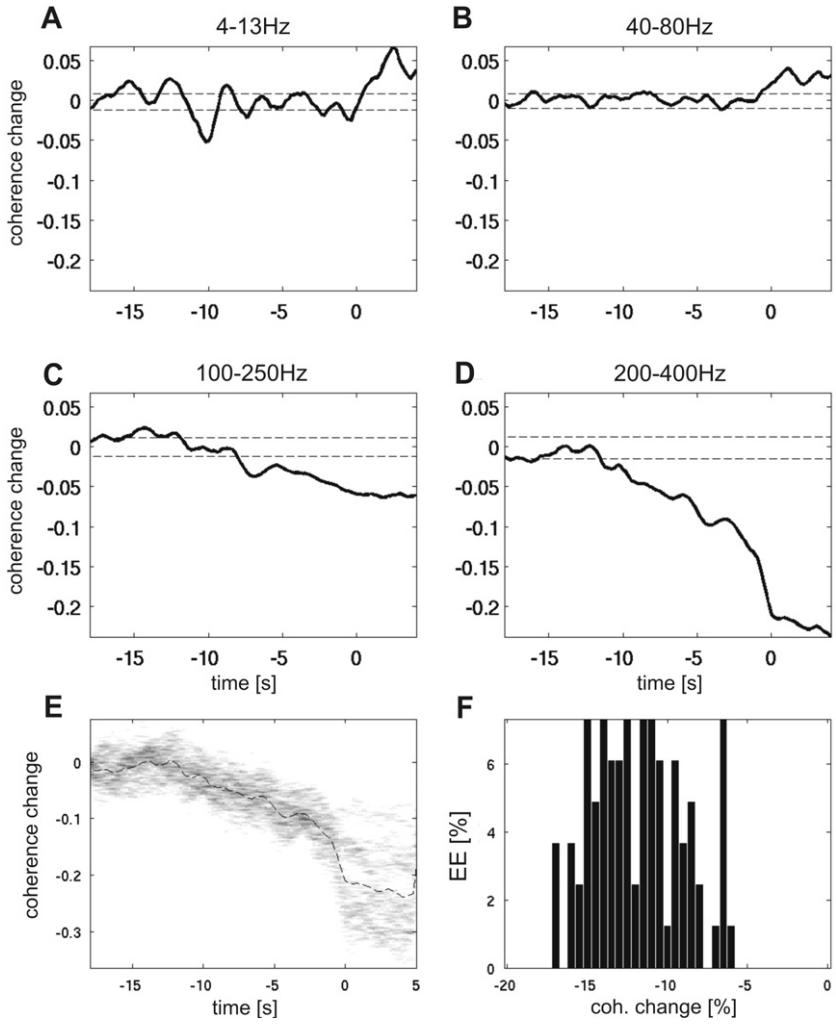

Fig. 5. The time-resolved relative changes of coherence before long EEs were more pronounced than those before short EEs. Details as in Fig. 4. The decrease of coherence in ripple (C) and FR (D) frequency ranges was even more pronounced than for short EEs and crosses the 1 SD threshold earlier—about 9 s before EE onset for ripples and 12±3 s for FR. This decrease was significantly more pronounced ($p<0.0001$, Student's t-test) and significantly earlier ($p<0.0001$, Student's t-test) than for short EEs. Besides, at the onset of EEs, coherence increased above the 1 SD threshold in the theta (A) and gamma frequency band (B) during the EE, matching the concomitant spiking. (E) All long EEs showed a decrease of coherence preceding the onset, however, the decrease at EE onset differed across the EEs. (F) The decrease of coherence was distributed around a mean of 12% (SD 2.9%) at 1 s before EE onset.

compared between baseline and 1 s before EE onset were quite similar and approximately normally distributed with a mean of 8% decrease (SD 1.8%) below baseline (Fig. 4F).

Generally, the changes of coherence observed for long EEs (Fig. 5) resembled those for short EEs (Fig. 4). In the theta range, EE onset was not preceded by significant changes of coherence, however, coherence increased above the 1 SD threshold at onset and remained increased throughout the EE (Fig. 5A), matching the observation of concomitant spiking in the ipsi- and contralateral hippocampus (Fig. 2A). In the gamma range, coherence likewise increased above mean + 1 SD at EE onset (Fig. 5B). As for short EEs, coherence decreased significantly at high frequencies (>100 Hz) preceding long EEs (Figs. 5C, D). This decrease, however, started even earlier and was more pronounced for long EEs than for short EEs. In the ripple range, the coherence decrease crossed the significance threshold approximately 9 s before EE onset (Fig. 5C). Coherence then further decreased until EE onset and remained at this low level for the first 5 s of the EE. Since we focused on processes preceding EEs, we did not investigate the coherence development for longer duration during the EEs. In the FR range, the coherence decrease was even more pronounced and crossed the significance threshold already 12±3 s before EE onset (Fig. 5D) and then decreased even further. Also here, the crossing of the mean + 1 SD threshold was significantly earlier than for short EEs ($p<0.0001$, Student's t-test). A very pronounced further decrease with a steep slope was also observed with a small jitter immediately before EE onset. Directly after EE onset, a plateau was reached and coherence remained at the decreased level for the first 5 s of the EE. As for short EEs, this decrease of coherence occurred across all EEs (Fig. 5E) and with a mean of 12% decrease (SD 2.9%) at 1 s before EE onset (Fig. 5F). The decrease for long EEs was significantly more pronounced than for short EEs (Figs. 4F, 5 F, $p<0.0001$, Student's t-test).

In summary, phase coupling between the hippocampi decreased significantly several seconds before EE onset for all EEs and all mice, in particular at high frequencies. Furthermore, it was increased during EEs at low frequencies.

Signature of EE onset in frequency power

Power spectral density in relation to EE onset

The changes of coherence could result from either (i) mechanisms that desynchronize the two hippocampi preceding and during the build-up of EEs or (ii) changes of signal power

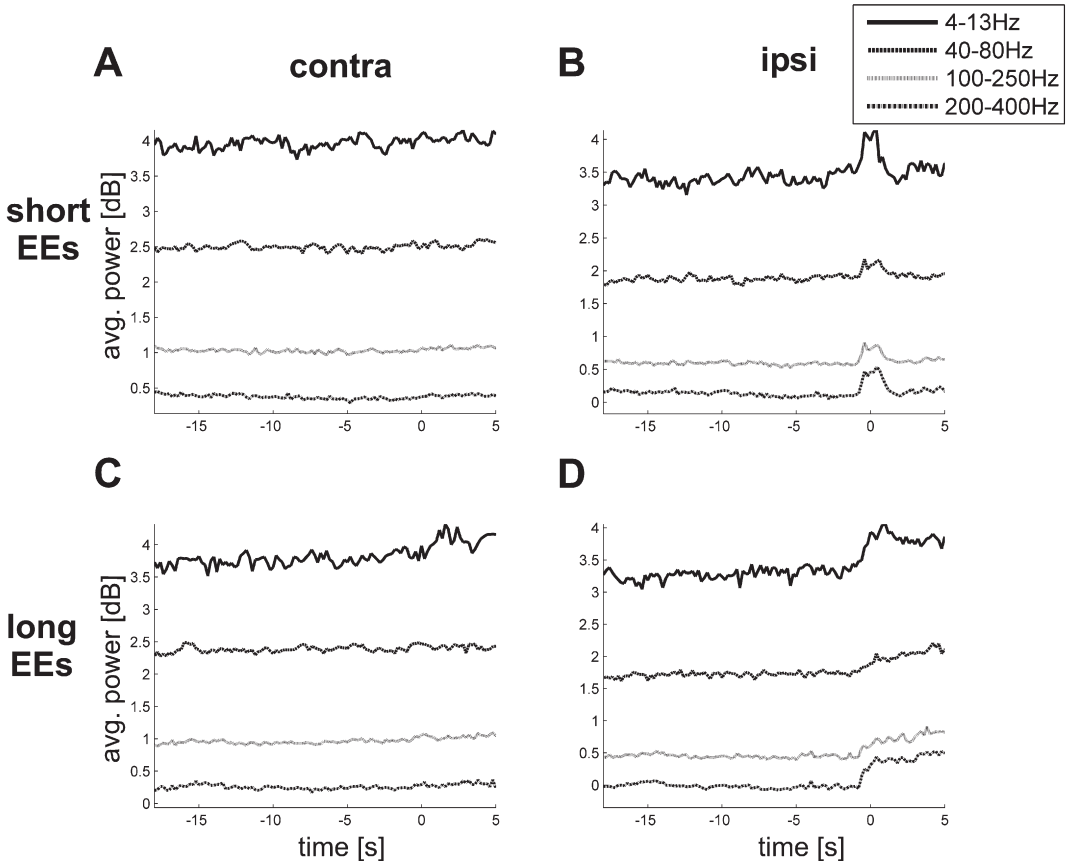

Fig. 6. Spectral power remained constant before EE onset and changed only at EE onset. Averaged absolute power spectral densities (PSDs) aligned to EE onset (on x-axis, time 0 s) are shown for four different frequency ranges: theta (4–13 Hz, solid line), gamma (40–80 Hz, dashed line), ripples (100–250 Hz, dotted line), and FR (200–400 Hz, dashed dotted line). (A, B) PSDs from short EEs, (A) in the contralateral, (B) in the ipsilateral hippocampus. (C, D) PSDs from long EEs, (C) in the contralateral, (D) in the ipsilateral hippocampus. The PSDs were flat before EE onset for all conditions, without any significant change of power across all frequency bands. On the ipsilateral side, a clear increase in power in all frequency bands at EE onset, lasting as long as the EEs, was observed. Smaller, but still visible, similar effects could be seen in the theta band for long EEs on the contralateral side (C).

preceding EE onset. We therefore analyzed the time course of the signal power during the time periods preceding EE onset for all aforementioned frequency bands.

In the ipsilateral hippocampus, time-resolved spectra showed changes in power concomitant with EE onset for short (Fig. 6B) and long EEs (Fig. 6D). During the 20 s preceding EE onset, however, no changes in power could be observed. At the onset of short EEs (Fig. 6B), spectral power increased substantially in the theta frequency band (4–13 Hz), as expected due to the high amplitude hypersynchronous spikes. Here, power also increased in gamma (40–80 Hz), ripple (100–250 Hz) and FR (200–400 Hz) ranges, most likely reflecting the multiunit ripples or FR riding on hypersynchronous spikes (Fig. 2D). The increase in power lasted for 2 s and then returned to baseline values, corresponding to the defined duration of short EEs. At the onset of long EEs (Fig. 6D), power increased in the theta range at onset. In contrast, in the gamma band, power increased not only at EE onset, but increased further during the first seconds of the ongoing EE. For ripple and FR bands, power also increased markedly at EE onset. Power remained increased for all frequency bands during the first 3 s of the EE.

In contrast, during short EEs power did not increase in the contralateral hippocampus (Fig. 6A) for any frequency band, suggesting that most of the short EEs did not propagate to the contralateral hippocampus. During long EEs (Fig. 6C), only power in the theta range was increased in the contralateral hippocampus corresponding to high amplitude spikes. In this frequency range, power thus changed differently in the ipsi- and contralateral hippocampus during, but not before EEs. Therefore, changes in coherence, presumably reflecting the interaction of activity between the hippocampi, are rather due to changes in bilateral synchrony than dependent on a simple modulation of signal power preceding the onset of EEs.

Accuracy of EE onset detection and spectral structure preceding EE onset

Since we determined the EE onset by visual inspection, possible misalignment of data or systematically distributed hidden (pre)-EE structures could interfere with the analysis at EE onset. To identify possible data structures that could interfere with our analyses, we used a data mining approach for unsupervised hierarchical clustering of the power spectral density in peri-EE time bins.

MANOVA-based single-link clustering of power spectral density in time bins preceding EE onset and during the first 5 s after onset would reveal errors in EE onset definition or its detection. Fig. 7 shows dendrograms based on the average Euclidian distance between time bins relative to EE onset. Two clearly distinct clusters are visible. One group holds all time bins before the defined EE onset (−19 s to −2 s), without sequential order within this group. The second group captures all time bins during EEs and immediately preceding EE onset (−1 s to 3 s). This separation into two clusters was prevalent for data both from the ipsi- and the contralateral hippocampus. The inter-cluster distances in the ipsilateral hippocampus (Fig. 7A, ordinate), however, were larger (approximately 6 times) than in the contralateral hippocampus (Fig. 7B, ordinate, enlarged in C). The finding that the −1-s time bin clustered into the EE time bins indicates a small jitter of maximally 1 s in onset detection. This was, however, much smaller than the time range of changes of

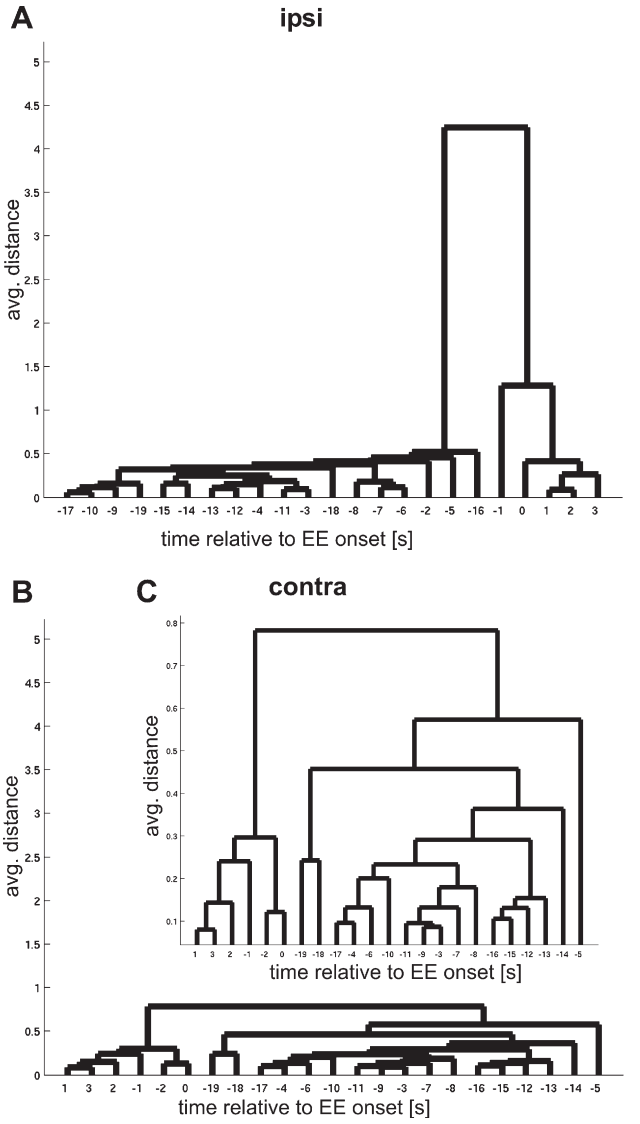

Fig. 7. MANOVA-based single-link clustering confirmed both the validity of EE detection based on visual inspection and the lack of patterns in the power spectrum before the onset of long EEs. The *y*-axis gives the average group distance. Time bins are labeled according to the first sample they contain, i.e., "−1" starts 1 s before EE onset and ends exactly at EE onset. Therefore, a jitter smaller than 1 s in onset detection may have contributed to the −1 s values in Figs. 4 and 5. (A) Clustering for the data from the ipsilateral hippocampus. Two significant clusters were visible, grouping onset and EE data into one group (the time bins −1 to 3; right side of the *x*-axis), and pre-EE bins (−19 to −2) into another. No clustering was visible within the strictly pre-EE group (−19 to −2). (B) Data from the contralateral hippocampus showed similar clustering as data from the ipsilateral hippocampus, but with a much lower signal to noise ratio (visible as overall lower average group distances). An enlarged plot of panel B is given in panel C. Again, the biggest clusters separate pre-EE time bins from EE time bins.

coherence preceding EEs (Figs. 4, 5). This small jitter in onset detection could also contribute to the sharp decrease of coherence just before EE onset (Figs. 4D, 5D). EEs are therefore separable from baseline activity based on a marked change of frequency power at EE onset. In particular, there was no visible pattern in the pre-EE time-resolved power spectrum. This further strengthens our finding that there is no significant modulation in single channel

LFP power preceding EE. Moreover, this analysis on a broad frequency band demonstrates that we consistently marked EE onset with accuracy better than 1 s.

Discussion

In this study we analyzed the network dynamics associated with EE initiation and we therefore focused on the few seconds of activity preceding EE onset.

Using the kainate model for MTLE in mice, our results show that, in addition to the ipsilateral, histologically changed hippocampus, epileptic discharges also occur in the contralateral, presumably intact hippocampus. We show that EE onset could be clearly identified and was neither preceded by changes in firing frequency of single spikes, their synchrony over EEs or the irregularity of the spike patterns nor by changes in power spectral density. Coherence between the two hippocampi increased in the theta and gamma frequency bands during long EEs, matching the concomitant spiking. More importantly, several seconds before EE onset coherence between the two hippocampi decreased significantly and highly stable across all EEs and all mice at high frequencies (>100 Hz), seemingly revealing an essential seizure initiation process, even though no obvious changes could be observed in the raw LFP data.

The contralateral hippocampus participates in epileptiform events

In previous studies in the same mouse model for MTLE it was shown that the early status epilepticus after kainate injection occurred in both the ipsi- and contralateral hippocampus, while later EEs were confined to the ipsilateral hippocampus (Riban et al., 2002). In a recent study using this model, spikes in the contralateral hippocampus concomitant with EEs in the ipsilateral hippocampus were mentioned for some animals, although no data were shown (Arabadzisz et al., 2005). The same study suggested increased inhibition and decreased excitation of CA3 in the contralateral hippocampus that might prevent the formation of an independent epileptic focus.

In our study, we observed spikes in the contralateral hippocampus concomitant with those in the ipsilateral hippocampus during EEs in all mice, but starting with a mean delay of 24 ms. Although very short EEs were rarely visible in the contralateral hemisphere, longer EEs were always observed. Due to the high interconnectivity between the hippocampi in rodents, a propagation of EEs from the ipsilateral to the contralateral hippocampus would be quite likely. Yet, following kainate injections, cells with commissural projections to the contralateral hippocampus degenerate, among those especially mossy cells and inhibitory cells in the hilus (Bouilleret et al., 1999; Riban et al., 2002). The degree of hippocampal sclerosis, however, appears to decrease with distance from the injection site in this model (data not shown), suggesting that commissural projections still exist at this level. Indeed, preliminary results indicate that epileptiform activity spreads in septotemporal direction in the injected hippocampus (data not shown). EEs could, thus, propagate to the contralateral hippocampus via less affected ipsilateral areas. In addition we did not observe the formation of an independent "mirror focus" during the course of our experiments, in agreement with previous reports (Riban et al., 2002; Arabadzisz et al., 2005). Finally, our observation of spiking in both hippocampi, with FR activity riding on epileptic spikes only in the ipsilateral hippocampus, matches findings in rats with intrahippocampal kainate injections (Bragin et al., 2002, 2005).

Coherence changes precede the onset of epileptiform events

The concomitant spiking in both hippocampi suggests that they might not only interact during EEs, but also in their generation. We therefore analyzed the synchronization of activity in the two hippocampi prior to EE onset using a coherence analysis method in concordance with previously reported methods (Thatcher et al., 2005; Poulos et al., 2004).

Here, we analyzed trends of coherence with respect to the onset of EEs during a 20-s baseline period. In addition, we extended the analysis to high-frequency bands that could more directly reflect the spiking activity in the underlying network. Increased coherence in theta and gamma frequencies during long EEs indicated that epileptiform spikes are tightly coupled between the hippocampi, likely due to propagation pathways with constant delays. A more striking observation was, however, the dynamics of coherence before the onset of EEs from 100 to 400 Hz. Coherence decreased significantly several seconds before the onset of EEs, indicating a decoupling of the bilateral activity dynamics in the two hippocampi. The threshold of mean+1 SD was crossed approximately 4 s earlier for long EEs than for short EEs and the full extent of the decrease was stronger preceding long EEs. This difference in extent was reliable and the decrease across EEs was approximately normally distributed. Short and long EEs thus seem to share common mechanisms, yet the resulting duration of the EEs was different and seems to be correlated with the onset and extent of decoupling. Thus, we hypothesize that short and long EEs differ in the amount of network recruited into EE generation.

Based on the temporal structure of the decoupling of the hippocampi, various processes affecting the network dynamics can be hypothesized. In contrast to analyses that aim to predict seizures as early as possible (Mormann et al., 2007; Iasemidis et al., 2005), e.g., for pharmacological intervention, the goal of understanding the mechanisms leading to the seizure proper at the cellular level requires the analysis of the short-term dynamics unbalancing the system. In simulation studies, disturbances of the network connectivity, such as changes in the relative size of excitatory and inhibitory cell populations or recurrent connectivity, increased the disposition for hypersynchronization in the hippocampus (Santhakumar et al., 2005). In the intrahippocampal kainate model in mice, the contralateral hippocampus was suggested to increase the overall inhibition and decrease excitation of CA3, which may counterbalance the overexcitation through recurrent connectivity of granule cells due to mossy fiber sprouting (Arabadzisz et al., 2005). Additionally, it has been shown in kainate-injected rats that recurrent mossy fibers simultaneously activate inhibitory cells in the dentate gyrus (Sloviter et al., 2006). Although these processes changing the hippocampal connectivity could explain the overall reduced coherence between the hippocampi in the kainate mouse model (Arabadzisz et al., 2005), they are not sufficient to account for the further decrease of coherence that we observed during the initiation phase of EEs.

The decrease of coherence immediately preceding EEs in our analysis is most prominent at high frequencies. LFPs at high frequencies are associated with gap junctions (Nimmrich et al., 2005). It has been suggested that functional changes in gap junctions are crucial for the initiation and maintenance of seizures

(Traub, 2003; Traub et al., 2001). Gap junction function depends on a variety of external factors, like pH and blood oxygenation levels (Perez Velazquez and Carlen, 2000). These factors can change on a time scale of several seconds, e.g., when seizures are triggered by hyperventilation (Guaranha et al., 2005). This time scale is in the same order of magnitude as the decoupling process of the two hippocampi we observed and, thus, the aforementioned factors might serve as a possible underlying mechanism influencing and possibly disbalancing the network dynamics, ultimately giving rise to an EE.

To determine whether the contralateral hippocampus is an essential component of the initiation process of seizures, either the separation of the two hippocampi or the measurement of the two hippocampi *ex vivo*, a technique demonstrated in young rats (Khalilov et al., 2003) would be necessary. The necessity of the interaction of sclerotic tissue with healthy tissue for EE generation is supported by the finding that in the kainate model in rats the ipsilateral sclerotic hippocampus is hyperinhibited, instead of being hyperexcitable (Frotscher et al., 2006; Sloviter et al., 2006). Although increased inhibition has been shown to be fragile (Wu and Leung, 2001), a mechanism for seizure related shut down of inhibition is not yet known. Despite the major differences between the kainate model in rats and mice, the aforementioned findings support our hypothesis that the sclerotic areas of the hippocampus are unlikely to generate hypersynchronizing activity independently. Thus, interaction with other brain areas like the contralateral hippocampus and/or other intact areas of the ipsilateral hippocampus or the entorhinal cortex seems to be required for seizure generation.

In the present study we demonstrate highly reliable changes in coherence between the two hippocampi several seconds before EE onset. The reliability of the bilateral decoupling observed in our study suggests that, besides the changes in the network, connectivity developing on a long time range short-term network mechanisms exists, that ultimately initiate epileptiform dynamics. Our study indicates a highly reliable time range of 8–12 s before EE onset for these dynamics, thus limiting the window for further investigations, like recording of single cell spiking or development of oxygen concentration in the tissue with respect to seizure onset. Additionally, our data suggest that the interactions between histologically changed and normal brain areas should be further explored to understand their role in seizure generation. Moreover, the observed short-term processes could be ideal targets to develop suitable pre-seizure intervention approaches to reestablish network balance and prevent EEs.

Acknowledgments

This work was supported by the German Federal Ministry of Education and Research (BMBF grant 01GQ0420 to BCCN Freiburg), INSERM, Fondation pour la Recherche Medicale, Fondation de l'Avenir and DAAD (U.H.). We would like to thank George Gerstein for the helpful comments on earlier versions of this manuscript.

References

Arabadzisz, D., Antal, K., Parpan, F., Emri, Z., Fritschy, J.M., 2005. Epileptogenesis and chronic seizures in a mouse model of temporal lobe epilepsy are associated with distinct EEG patterns and selective neurochemical alterations in the contralateral hippocampus. Exp. Neurol. 194, 76–90.

Bouilleret, V., Ridoux, V., Depaulis, A., Marescaux, C., Nehlig, A., Le Gal, L.S., 1999. Recurrent seizures and hippocampal sclerosis following intrahippocampal kainate injection in adult mice: electroencephalography, histopathology and synaptic reorganization similar to mesial temporal lobe epilepsy. Neuroscience 89, 717–729.

Bragin, A., Engel Jr., J., Wilson, C.L., Fried, I., Mathern, G.W., 1999. Hippocampal and entorhinal cortex high-frequency oscillations (100–500 Hz) in human epileptic brain and in kainic acid-treated rats with chronic seizures. Epilepsia 40, 127–137.

Bragin, A., Mody, I., Wilson, C.L., Engel Jr., J., 2002. Local generation of fast ripples in epileptic brain. J. Neurosci. 22, 2012–2021.

Bragin, A., Azizyan, A., Almajano, J., Wilson, C.L., Engel Jr., J., 2005. Analysis of chronic seizure onsets after intrahippocampal kainic acid injection in freely moving rats. Epilepsia 46, 1592–1598.

Buzsaki, G., Buhl, D.L., Harris, K.D., Csicsvari, J., Czeh, B., Morozov, A., 2003. Hippocampal network patterns of activity in the mouse. Neuroscience 116, 201–211.

Cendes, F., Kahane, P., Brodie, M., Andermann, F., 2002. The mesiotemporal lobe epilepsy syndrome. In: Roger, J., Bureau, M., Dravet, C., Genton, P., Tassinari, C.A., Wolf, P. (Eds.), Epileptic Syndromes in Infancy, Childhood and Adolescence. John Libbey and Company, Eastleigh, UK, pp. 513–530.

Chabardes, S., Kahane, P., Minotti, L., Tassi, L., Grand, S., Hoffmann, D., Benabid, A.L., 2005. The temporopolar cortex plays a pivotal role in temporal lobe seizures. Brain 128, 1818–1831.

Chatfield, C., 1999. The Analysis of Time Series. An Introduction (Texts in Statistical Science), fifth ed. CRC-press reprints–Boca Raton: Chapman and Hall.

Deller, T., Nitsch, R., Frotscher, M., 1995. Phaseolus vulgaris-leucoagglutinin tracing of commissural fibers to the rat dentate gyrus: evidence for a previously unknown commissural projection to the outer molecular layer. J. Comp. Neurol. 352, 55–68.

Engel Jr., J., 1996. Introduction to temporal lobe epilepsy. Epilepsy Res. 26, 141–150.

Fano, U., 1947. Ionization yield of radiations: II. The fluctuations of the number of ions. Phys. Rev. 72 (1), 26–29.

Frotscher, M., Seress, L., Schwerdtfeger, W.K., Buhl, E., 1991. The mossy cells of the fascia dentata: a comparative study of their fine structure and synaptic connections in rodents and primates. J. Comp. Neurol. 312, 145–163.

Frotscher, M., Jonas, P., Sloviter, R.S., 2006. Synapses formed by normal and abnormal hippocampal mossy fibers. Cell Tissue Res. 326 (2), 361–367.

Guaranha, M.S., Garzon, E., Buchpiguel, C.A., Tazima, S., Yacubian, E.M., Sakamoto, A.C., 2005. Hyperventilation revisited: physiological effects and efficacy on focal seizure activation in the era of video-EEG monitoring. Epilepsia 46, 69–75.

Heinrich, C., Nitta, N., Flubacher, A., Muller, M., Fahrner, A., Kirsch, M., Freiman, T., Suzuki, F., Depaulis, A., Frotscher, M., Haas, C.A., 2006. Reelin deficiency and displacement of mature neurons, but not neurogenesis, underlie the formation of granule cell dispersion in the epileptic hippocampus. J. Neurosci. 26, 4701–4713.

Iasemidis, L.D., Shiau, D.S., Pardalos, P.M., Chaovalitwongse, W., Narayanan, K., Prasad, A., Tsakalis, K., Carney, P.R., Sackellares, J.C., 2005. Long-term prospective on-line real-time seizure prediction. Clin. Neurophysiol. 116, 532–544.

Jain, A., Murty, M., Plynn, P., 1999. Data clustering: a review. ACM Comput. Surv. 31 (Nr 3) (September), 264–323.

Khalilov, I., Holmes, G.L., Ben Ari, Y., 2003. In vitro formation of a secondary epileptogenic mirror focus by interhippocampal propagation of seizures. Nat. Neurosci. 6, 1079–1085.

Krzanowski, W.J., 1988. Principles of Multivariate Analysis. Oxford Univ. Press.

Laurberg, S., Sorensen, K.E., 1981. Associational and commissural collaterals of neurons in the hippocampal formation (hilus fasciae dentate and subfield CA3). Brain Res. 212, 287–300.

Mormann, F., Kreuz, T., Andrzejak, R.G., David, P., Lehnertz, K., Elger,

C.E., 2003. Epileptic seizures are preceded by a decrease in synchronization. Epilepsy Res. 53, 173–185.
Mormann, F., Andrzejak, R.G., Elger, C.E., Lehnertz, K., 2007. Seizure prediction: the long and winding road. Brain 130, 314–333.
Nimmrich, V., Maier, N., Schmitz, D., Draguhn, A., 2005. Induced sharp wave-ripple complexes in the absence of synaptic inhibition in mouse hippocampal slices. J. Physiol. 563, 663–670.
Nunez, P.L., Srinivasan, R., Westdorp, A.F., Wijesinghe, R.S., Tucker, D. M., Silberstein, R.B., 1997. EEG coherency: I. Statistics, reference electrode, volume conduction, Laplacians, cortical imaging, and interpretation at multiple scales. Electroencephalogr. Clin. Neurophysiol. 103, 499–515.
Nunez, P.L., Silberstein, R.B., Shi, Z., Carpenter, M.R., Srinivasan, R., Tucker, D.M., Doran, S.M., Cadusch, P.J., 1999. EEG coherency: II. Experimental comparisons of multiple measures. Clin. Neurophysiol. 110, 469–486.
Perez Velazquez, J.L., Carlen, P.L., 2000. Gap junctions, synchrony and seizures. Trends Neurosci. 23, 68–74.
Poulos, M., Papavlasopoulos, S., Alexandris, N., Vlachos, E., 2004. Comparison between auto-cross-correlation coefficients and coherence methods applied to the EEG for diagnostic purposes. Med. Sci. Monit. 10, MT99–MT108.
Priestley, M.B., 1982. Spectral Analysis and Time Series. Elsevier, Amsterdam, Heidelberg.
Quiroga, R.Q., Nadasdy, Z., Ben-Shaul, Y., 2004. Unsupervised spike detection and sorting with wavelets and superparamagnetic clustering. Neural Comput. 16, 1661–1687.
Rappelsberger, P., Pfurtscheller, G., Filz, O., 1994. Calculation of event-related coherence—A new method to study short-lasting coupling between brain areas. Brain Topogr. 7, 121–127.
Ribak, C.E., Seress, L., Amaral, D.G., 1985. The development, ultrastructure and synaptic connections of the mossy cells of the dentate gyrus. J. Neurocytol. 14, 835–857.
Riban, V., Bouilleret, V., Pham, L., Fritschy, J.M., Marescaux, C., Depaulis, A., 2002. Evolution of hippocampal epileptic activity during the development of hippocampal sclerosis in a mouse model of temporal lobe epilepsy. Neuroscience 112, 101–111.
Rieke, F., de Ruyter van Steveninck, R., Bialek, W., 1997. Spikes: Exploring the Neural Code. The MIT Press.
Santhakumar, V., Aradi, I., Soltesz, I., 2005. Role of mossy fiber sprouting and mossy cell loss in hyperexcitability: a network model of the dentate gyrus incorporating cell types and axonal topography. J. Neurophysiol. 93, 437–453.
Sloviter, R.S., Zappone, C.A., Harvey, B.D., Frotscher, M., 2006. Kainic acid-induced recurrent mossy fiber innervation of dentate gyrus inhibitory interneurons: possible anatomical substrate of granule cell hyper-inhibition in chronically epileptic rats. J. Comp. Neurol. 494, 944–960.
Suzuki, F., Junier, M.P., Guilhem, D., Sorensen, J.C., Onteniente, B., 1995. Morphogenetic effect of kainate on adult hippocampal neurons associated with a prolonged expression of brain-derived neurotrophic factor. Neuroscience 64, 665–674.
Swanson, L.W., Wyss, J.M., Cowan, W.M., 1978. An autoradiographic study of the organization of intrahippocampal association pathways in the rat. J. Comp. Neurol. 181, 681–715.
Thatcher, R.W., North, D., Biver, C., 2005. EEG and intelligence: relations between EEG coherence, EEG phase delay and power. Clin. Neurophysiol. 116, 2129–2141.
Traub, R.D., 2003. Fast oscillations and epilepsy. Epilepsy Curr. 3, 77–79.
Traub, R.D., Whittington, M.A., Buhl, E.H., Lebeau, F.E., Bibbig, A., Boyd, S., Cross, H., Baldeweg, T., 2001. A possible role for gap junctions in generation of very fast EEG oscillations preceding the onset of, and perhaps initiating, seizures. Epilepsia 42, 153–170.
Wieser, H.G., 2004. ILAE Commission Report. Mesial temporal lobe epilepsy with hippocampal sclerosis. Epilepsia 45, 695–714.
Wu, K., Leung, L.S., 2001. Enhanced but fragile inhibition in the dentate gyrus *in vivo* in the kainic acid model of temporal lobe epilepsy: a study using current source density analysis. Neuroscience 104, 379–396.